

A NON-SPURIOUS VECTOR SPECTRAL ELEMENT METHOD FOR MAXWELL'S EQUATIONS

J. Chen and Q. H. Liu

Department of Electrical and Computer Engineering
Duke University
Durham, NC 27708, USA

Abstract—In this paper, a non-spurious vector spectral element method is proposed to solve Maxwell's equations using \mathbf{E} and \mathbf{H} as variables. The mixed-order curl-conforming basis functions are used for both variables to facilitate applying boundary and interface conditions; and the interpolation degree of basis functions for \mathbf{E} is set different from that for \mathbf{H} to suppress the spurious modes. The proposed method can be utilized in both time domain and frequency domain, and it is very suitable for the future implementation of discontinuous Galerkin spectral element method. Numerical results demonstrate the property of spurious-free and the spectral accuracy of this method. The method has also been implemented for the more general finite element method in time and frequency domains.

1. INTRODUCTION

The discontinuous Galerkin spectral element method (DG-SEM) and collocation method [1–7] are promising methods to simulate multiscale electromagnetic problems, wherein electrically large and electrically small structures coexist. They can divide a whole system into several subdomains based on its material distribution and geometric characteristics, and they can choose spectral element (SEM) [8–12] or spectral collocation (such as the discontinuous Galerkin pseudospectral time-domain method in [6]) with different interpolations orders to simulate different subdomains, thus making an optimized spatial discretization scheme and achieving high accuracy with a relatively small number of unknowns.

Corresponding author: Q. H. Liu (qhliu@ee.duke.edu).

There are two types of SEM for computational electromagnetics: One is based on the second order wave equation and the other is based on the first order Maxwell's equations. As to the aim of implementation of DG-SEM, the second version of SEM is superior to the first one because the numerical fluxes such as the Riemann solver [13], which are the critical parts used in DG-SEM to communicate and correct fields between different subdomains, are defined by tangential components of \mathbf{E} and \mathbf{H} on the interfaces between subdomains. To construct a robust DG-SEM for electromagnetic problems, a non-spurious SEM scheme based on variables \mathbf{E} and \mathbf{H} for the first order Maxwell's equations is in demand.

While it is well-known that the employment of mixed-order curl-conforming vector basis function can make a SEM scheme based on the second order wave equation free of spurious modes [14], the same technique, viz. merely using vector basis functions for both \mathbf{E} and \mathbf{H} cannot guarantee a non-spurious SEM scheme for the first order Maxwell's equations [15]. Based on our numerical experiments, we find that to construct non-spurious vector spectral element schemes for Maxwell's equations, the interpolation order of vector basic functions for \mathbf{E} is required to be different from that for \mathbf{H} . To the best of our knowledge, this is the first non-spurious vector spectral element method for Maxwell's equations based on the variables \mathbf{E} and \mathbf{H} . Numerical results confirm our conclusion.

2. FORMULATION AND ALGORITHM

Consider the first order Maxwell's equations

$$\epsilon \frac{\partial \mathbf{E}}{\partial t} = \nabla \times \mathbf{H} - \sigma \mathbf{E} - \mathbf{J}_s(\mathbf{r}, t) \quad (1)$$

$$\mu \frac{\partial \mathbf{H}}{\partial t} = -\nabla \times \mathbf{E} \quad (2)$$

where \mathbf{E} and \mathbf{H} are the electric and magnetic fields; \mathbf{J}_s is applied electric current densities; ϵ , μ , and σ denote material's permittivity, permeability, and electric conductivity, respectively. We use the mixed-order curl-conforming vector spectral elements [10, 11] to discretize both \mathbf{E} and \mathbf{H} in Maxwell's equations. Denote $\hat{\mathbf{\Phi}}^{(M)}$ as the vector basis function for \mathbf{E} with M -th order of interpolation, we have

$$\begin{cases} \xi \hat{\mathbf{\Phi}}_{mnp}^{(M)} = \hat{\xi} \phi_m^{(M-1)}(\xi) \phi_n^{(M)}(\eta) \phi_p^{(M)}(\zeta) \\ \eta \hat{\mathbf{\Phi}}_{mnp}^{(M)} = \hat{\eta} \phi_m^{(M)}(\xi) \phi_n^{(M-1)}(\eta) \phi_p^{(M)}(\zeta) \\ \zeta \hat{\mathbf{\Phi}}_{mnp}^{(M)} = \hat{\zeta} \phi_m^{(M)}(\xi) \phi_n^{(M)}(\eta) \phi_p^{(M-1)}(\zeta) \end{cases} \quad (3)$$

where

$$\phi_m^{(M)}(\xi) = \frac{-(1 - \xi^2) L'_M(\xi)}{M(M + 1)L_M(\xi_m)(\xi - \xi_m)}, \quad m = 0, \dots, M \quad (4)$$

$L_M(\xi)$ is the Legendre polynomial of degree of M , and ξ_m is chosen as $(1 - \xi_m^2)L'_M(\xi_m) = 0$. $\phi_n^{(M)}(\eta)$ and $\phi_p^{(M)}(\zeta)$ are functions of η and ζ , respectively, and they have similar formulation as $\phi_m^{(M)}(\xi)$. The reference domain with coordinates ξ , η , and ζ is a standard cube $[-1, 1] \times [-1, 1] \times [-1, 1]$ mapped from an arbitrary curved hexahedron in the physical domain, and $\hat{\xi}$, $\hat{\eta}$, and $\hat{\zeta}$ denote the unit vectors along the corresponding directions.

The vector basis functions for \mathbf{H} are almost the same with the basis functions for \mathbf{E} . Take $\hat{\Psi}^{(N)}$ with N -th order of interpolation for instance

$$\begin{cases} \xi \hat{\Psi}_{mnp}^{(N)} = \hat{\xi} \phi_m^{(N-1)}(\xi) \phi_n^{(N)}(\eta) \phi_p^{(N)}(\zeta) \\ \eta \hat{\Psi}_{mnp}^{(N)} = \hat{\eta} \phi_m^{(N)}(\xi) \phi_n^{(N-1)}(\eta) \phi_p^{(N)}(\zeta) \\ \zeta \hat{\Psi}_{mnp}^{(N)} = \hat{\zeta} \phi_m^{(N)}(\xi) \phi_n^{(N)}(\eta) \phi_p^{(N-1)}(\zeta) \end{cases} \quad (5)$$

All arguments in (5) have the same meanings with those in (3) and (4).

Although both $\hat{\Phi}^{(M)}$ and $\hat{\Psi}^{(N)}$ are vector-based basis functions, spurious modes will still be generated under distorted meshes if the interpolation order for $\hat{\Phi}^{(M)}$ is set as the same with that for $\hat{\Psi}^{(N)}$. This is observed in our numerous numerical tests, and apparently has not been reported previously for the coupled Faraday's law and Ampère's law in electromagnetics (a similar phenomenon has been reported for mechanic problems in [16]). Based on our numerical experiments, we found that there is one more condition to be satisfied to construct a non-spurious vector spectral element method for Maxwell's equations: The interpolation order of $\hat{\Phi}^{(M)}$ must be different from that of $\hat{\Psi}^{(N)}$, i.e., $M \neq N$. A non-spurious SEM scheme for Maxwell's equations is shown in Fig. 1.

The Galerkin's weak forms of Maxwell's equations are

$$\begin{aligned} & \sum_{j=1}^{N_e} \frac{de_j}{dt} \int_{-1}^1 \int_{-1}^1 \int_{-1}^1 \hat{\Phi}_i^T \mathbf{J}^{-T} \epsilon \mathbf{J}^{-1} \hat{\Phi}_j |\mathbf{J}| d\xi d\eta d\zeta \\ & = \sum_{k=1}^{N_h} h_k \int_{-1}^1 \int_{-1}^1 \int_{-1}^1 \hat{\Phi}_i^T \left(\hat{\nabla} \times \hat{\Psi}_k \right) d\xi d\eta d\zeta \end{aligned}$$

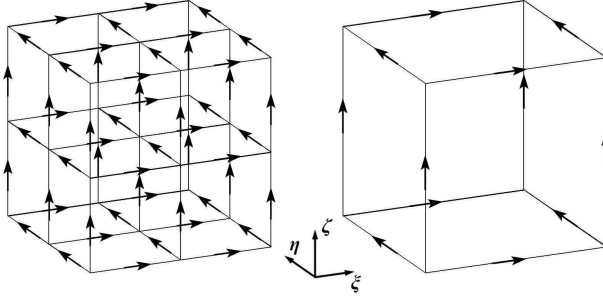


Figure 1. A non-spurious SEM scheme for the Maxwell's equations: (left) second order element for \mathbf{E} and (right) first order element for \mathbf{H} .

$$\begin{aligned}
 & - \sum_{j=1}^{N_e} e_j \int_{-1}^1 \int_{-1}^1 \int_{-1}^1 \hat{\Phi}_i^T \mathbf{J}^{-T} \sigma \mathbf{J}^{-1} \hat{\Phi}_j | \mathbf{J} | d\xi d\eta d\zeta \\
 & - \int_{-1}^1 \int_{-1}^1 \int_{-1}^1 \hat{\Phi}_i^T \mathbf{J}^{-T} \mathbf{J}_s | \mathbf{J} | d\xi d\eta d\zeta \quad i = 1, 2, \dots, N_e \quad (6)
 \end{aligned}$$

$$\begin{aligned}
 & \sum_{k=1}^{N_h} \frac{dh_k}{dt} \int_{-1}^1 \int_{-1}^1 \int_{-1}^1 \hat{\Psi}_l^T \mathbf{J}^{-T} \mu \mathbf{J}^{-1} \hat{\Psi}_k | \mathbf{J} | d\xi d\eta d\zeta \\
 & = - \sum_{j=1}^{N_e} e_j \int_{-1}^1 \int_{-1}^1 \int_{-1}^1 \hat{\Psi}_l^T \left(\hat{\nabla} \times \hat{\Phi}_j \right) d\xi d\eta d\zeta \quad l = 1, 2, \dots, N_h \quad (7)
 \end{aligned}$$

where N_e and N_h denote the numbers of unknowns of \mathbf{E} and \mathbf{H} . e_j and h_k are coefficients for $\hat{\Phi}_j$ and $\hat{\Psi}_k$, respectively.

By assembling all spectral elements we will obtain the discretized system of equations as

$$\begin{cases} \mathbf{M}_{ee} \frac{d\mathbf{e}}{dt} = \mathbf{C}_{ee} \mathbf{e} + \mathbf{K}_{eh} \mathbf{h} + \mathbf{q} \\ \mathbf{M}_{hh} \frac{d\mathbf{h}}{dt} = \mathbf{K}_{he} \mathbf{e} \end{cases} \quad (8)$$

where vectors \mathbf{e} , \mathbf{h} , and \mathbf{q} are discretized electric field, magnetic field, and excitation, respectively. The detailed expressions for the above system matrices \mathbf{M}_{ee} , \mathbf{M}_{hh} , \mathbf{K}_{eh} , \mathbf{K}_{he} , and \mathbf{C}_{ee} can be referred to [12].

The formulation (8) is a set of ordinary differential equations in the time domain. Several time stepping algorithms, such as the leapfrog scheme and the Runge-Kutta method can be utilized to solve this set of equations. Besides, with the time convention $d/dt \rightarrow j\omega$, we can easily transform (8) from the time domain into the frequency domain,

in which the spurious modes are easier to be distinguished in the form of eigenmodes, and the spectral accuracy of the proposed method itself is more convenient to be demonstrated because the numerical errors due to time integration will not be introduced into SEM in the frequency domain. In the next section, we will show some results by this non-spurious SEM in both time domain and frequency domain.

3. NUMERICAL RESULTS

Consider a $1\text{ cm} \times 0.5\text{ cm} \times 0.75\text{ cm}$ metallic cavity filled with air centered at the origin of coordinates. In order to show the spurious modes by other basis functions, we use a distorted hexahedral mesh to discretize this cavity, which is shown in Fig. 2. We choose two different SEM schemes to solve this problem: Scheme 1 is SEM with different interpolation orders for \mathbf{E} and \mathbf{H} ($M = 5, N = 4$ in this case), and scheme 2 is SEM with the same interpolation order for \mathbf{E} and \mathbf{H} ($M = 5, N = 5$ in this case).

We first place a dipole with polarization $-0.62\hat{x} + 0.62\hat{y} + 0.47\hat{z}$ at $(-0.014, -0.236, 0.011)\text{ cm}$, and give the first derivative of the Blackman-Harris window pulse [17] with characteristic frequency as 9.4 GHz on the dipole, so only the dominant mode can be stimulated. We use these two SEM schemes to discretize this problem and use the 4th order Runge-Kutta method for time stepping (with $\Delta t = 0.5\text{ ps}$). Fig. 3 shows the time-varying \mathbf{E}_y at $(0.174, 0.239, 0.174)\text{ cm}$ and the frequency components by the two SEM schemes. From which we find that only one mode is stimulated by scheme 1 and the corresponding time-varying results by scheme 1 agree well with the reference, while scheme 2 will stimulate a lot of spurious modes and lead the time domain results deviating greatly from the reference. Fig. 4 shows

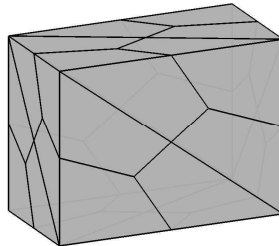


Figure 2. A distorted mesh for a metallic cavity, which has a dimension of $1\text{ cm} \times 0.5\text{ cm} \times 0.75\text{ cm}$ and is filled with vacuum.

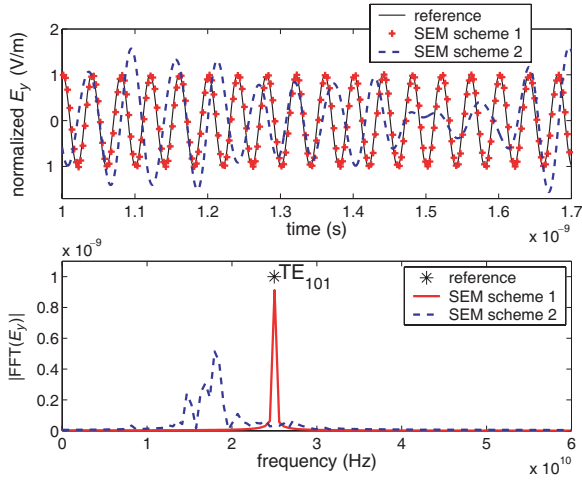


Figure 3. (upper) Time-varying \mathbf{E}_y on $(0.174, 0.239, 0.174)$ cm by two SEM schemes and (lower) corresponding frequency components after FFT.

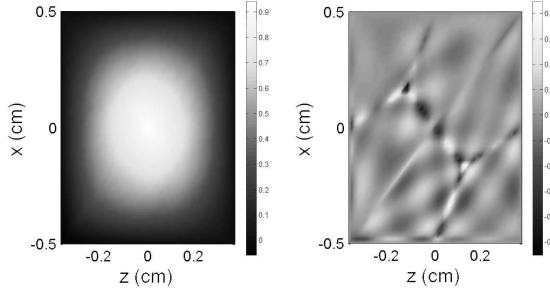


Figure 4. Snapshots of \mathbf{E}_y on the plane $y = 0$ at $t = 0.5$ ns (left) by SEM with different interpolation orders for \mathbf{E} and \mathbf{H} and (right) by SEM with the same interpolation order for \mathbf{E} and \mathbf{H} .

the snapshots of \mathbf{E}_y on the plane $y = 0$ at 1000-th time step ($t = 0.5$ ns). We observe that the field pattern by scheme 1 is consistent with the dominant mode (TE_{101}), while the results by scheme 2 are contaminated by spurious modes.

Then we use these two SEM schemes to solve the eigenvalue problem of this cavity in frequency domain. Fig. 5 shows the calculated eigenvalues by the two SEM schemes as well as analytical solutions, from which we find that the results by scheme 1 agree very well with analytical solutions, while scheme 2 generates many spurious eigenvalues between every two adjacent analytical eigenvalues.

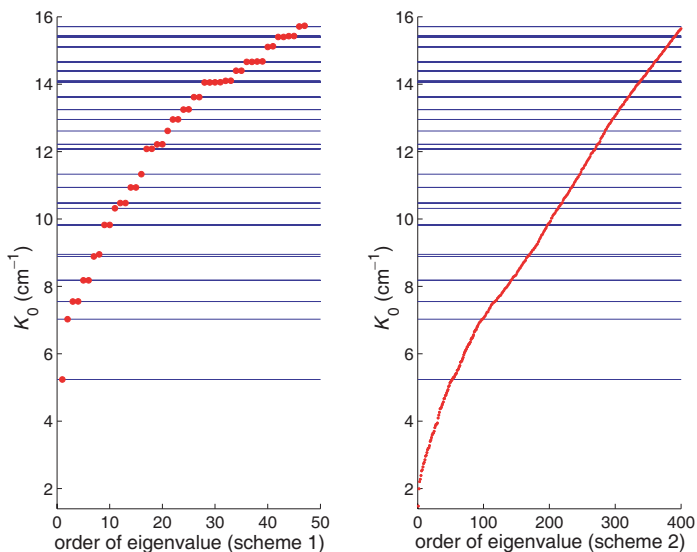


Figure 5. Eigenvalues of the cavity by SEM with different interpolation orders for \mathbf{E} and \mathbf{H} (left) and by SEM with the same interpolation order for \mathbf{E} and \mathbf{H} (right). The dots denote the calculated eigenvalues by SEM schemes and the horizontal lines denote analytical solutions.

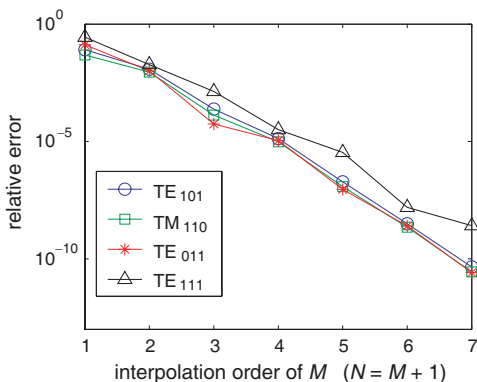


Figure 6. Errors of four modes of the metallic cavity by non-spurious SEM with different interpolation orders.

In Fig. 6, we plot the errors of four modes (TE_{101} , TM_{110} , TE_{011} , and TE_{111}) of this cavity by the non-spurious SEM with different interpolation orders of basis functions ($M = 1, 2, \dots, 7$, $N = M + 1$), from which we observe that the errors of all the four modes decrease

exponentially with the increase of interpolation order, i.e., the proposed non-spurious spectral element method can achieve spectral accuracy.

The second example is an open-region time-domain scattering problem with one dielectric cube and one PEC cube, both with a side length of 10 cm. The dielectric cube with $\epsilon_r = 4$ is centered at the origin, while the PEC cube is centered at (20, 20, 20) cm. The background medium in this example is air. A z -direction electric dipole is placed at the origin as the source, with the first derivative of the Blackman-Harris Window of characteristic frequency 1.55 GHz (i.e., with a pulse duration of 1 ns) as the time function [17]. Another z -direction dipole is placed at (11, 11, 11) cm as a receiver. A schematic of the second example is shown in Fig. 7.

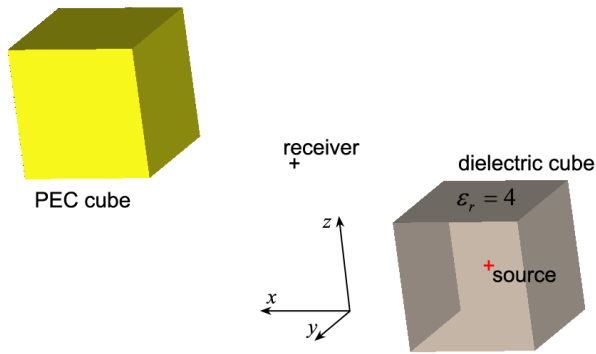


Figure 7. An open-region time-domain scattering problem with a $10\text{ cm} \times 10\text{ cm} \times 10\text{ cm}$ dielectric cube ($\epsilon_r = 4$) and a $10\text{ cm} \times 10\text{ cm} \times 10\text{ cm}$ PEC cube.

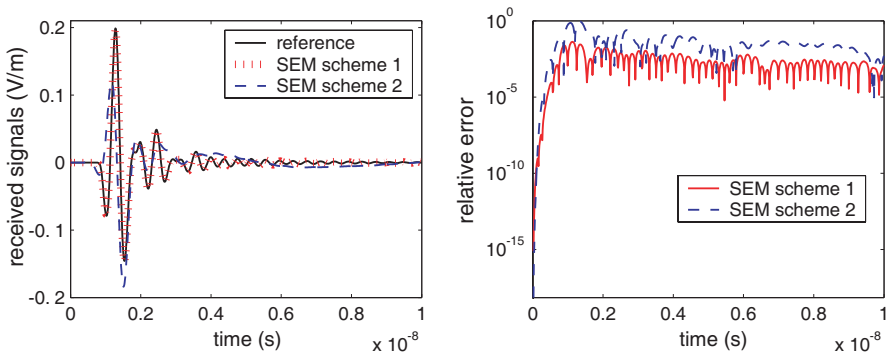


Figure 8. (left) Numerical results and (right) relative errors of timevarying received signals by the two SEM schemes.

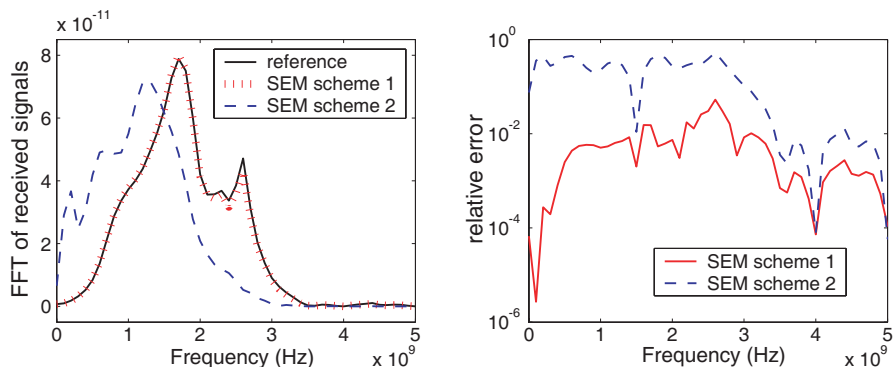


Figure 9. (left) Numerical results and (right) relative errors of frequency components of received signals by the two SEM schemes.

Two SEM schemes are chosen for the time-domain simulation of this problem. Scheme 1 is the SEM with different interpolation orders for \mathbf{E} and \mathbf{H} ($M = 2, N = 1$ in this case), and scheme 2 is the SEM with the same interpolation order for \mathbf{E} and \mathbf{H} ($M = 2, N = 2$ in this case). Since analytical solution is not available for this problem, numerical results by the finite-difference time-domain method enhanced by the enlarged cell technique in a commercial software, Wavenology EM [18], under a relatively dense grid are used as the reference. Fig. 8 shows the received time-varying signals by the two SEM schemes as well as the reference result and the relative errors. From these plots we observe that the result by SEM scheme 1 agrees well with the reference, while the result by SEM scheme 2 does not. Fig. 9 shows the comparison between numerical results and the reference in the frequency domain and the relative errors. From these figures we clearly observe good agreement between the result by SEM scheme 1 and the reference, while we find some spurious peaks in the low frequency regime from the result by SEM scheme 2. Based on these two figures, we can conclude that for an open-region problem, the SEM with different interpolation orders for \mathbf{E} and \mathbf{H} is a spurious-free scheme; however, the SEM scheme with same interpolation order for both \mathbf{E} and \mathbf{H} will generate spurious modes, and these spurious modes will contaminate time-domain and frequency-domain results.

Finally, a general rule of thumb is given for the choice of the order of basis functions in the non-spurious SEM. From many numerical tests we found that the mixed-vector SEM can be free of spurious modes as long as the interpolation degree for \mathbf{E} is different from that for \mathbf{H} . For the purpose of minimizing the difference between the number of unknowns for \mathbf{E} and that for \mathbf{H} , we set the difference between the

two interpolation degrees as 1. Furthermore, because PEC objects are more frequently encountered than PMC objects, we usually set the interpolation degree for \mathbf{E} one order higher than that for \mathbf{H} .

4. CONCLUSION

We propose a new non-spurious vector spectral element method for Maxwell's equations based on variables \mathbf{E} and \mathbf{H} . The mixed-order curl-conforming vector basis functions are employed to both variables, and the interpolation order of basis functions for \mathbf{E} is set different from that for \mathbf{H} . This SEM scheme is vector-based and spurious-free, and it can achieve spectral accuracy by increasing interpolation order of basis functions. The above properties make the proposed method very suitable for construction of DG-SEM, and this is in our current research. Furthermore, this scheme is applicable to and has been implemented for the more general finite element method in both time domain and frequency domain.

REFERENCES

1. Rasetarinera, P. and M. Y. Hussaini, "An efficient implicit discontinuous spectral Galerkin method," *J. Comput. Phys.*, Vol. 172, No. 2, 718–738, Sep. 2001.
2. Kopriva, D. A., S. L. Woodruff, and M. Y. Hussaini, "Computation of electromagnetic scattering with a non-conforming discontinuous spectral element method," *Int. J. Numer. Meth. Eng.*, Vol. 53, No. 1, 105–122, Oct. 2001.
3. Giraldo, F. X., J. S. Hesthaven, and T. Warburton, "Nodal high-order discontinuous Galerkin methods for the spherical shallow water equations," *J. Comput. Phys.*, Vol. 181, No. 2, 499–525, Sep. 2002.
4. Hesthaven, J. S. and T. C. Warburton, "Nodal high-order methods on unstructured grids — 1. Time-domain solution of Maxwell's equations," *J. Comput. Phys.*, Vol. 181, 186–221, 2002.
5. Xiao, T. and Q. H. Liu, "Three-dimensional unstructured-grid discontinuous Galerkin method for Maxwell's equations with well-posed perfectly matched layer," *Microwave Opt. Technol. Lett.*, Vol. 46, No. 5, 459–463, 2005.
6. Liu, Q. H. and G. Zhao, "Advances in PSTD techniques," *Computational Electrodynamics: The Finite-difference Time-domain Method*, A. Taflov and S. Hagness (eds.), Chapter 17, Artech House, Inc., 2005.

7. Shi, Y. and C.-H. Liang, "Simulations of the left-handed medium using discontinuous Galerkin method based on the hybrid domains," *Progress In Electromagnetics Research*, PIER 63, 171–191, 2006.
8. Kirsch, A. and P. Monk, "A finite element/spectral method for approximating the time-harmonic Maxwell system in \mathbb{R}^3 ," *SIAM Journal on Applied Mathematics*, Vol. 55, No. 5, 1324–1344, Oct. 1995.
9. Pingenot, J., R. N. Rieben, D. A. White, and D. G. Dudley, "Full wave analysis of RF signal attenuation in a lossy rough surface cave using a high order time domain vector finite element method," *Journal of Electromagnetic Waves and Applications*, Vol. 20, No. 12, 1695–1705, 2006.
10. Cohen, G., *Higher-order Numerical Methods for Transient Wave Equations*, Springer, Berlin, 2002.
11. Lee, J. H., T. Xiao, and Q. H. Liu, "A 3-D spectral-element method using mixed-order curl conforming vector basis functions for electromagnetic fields," *IEEE Trans. Microw. Theory Tech.*, Vol. 54, No. 1, 437–444, Jan. 2006.
12. Lee, J. H. and Q. H. Liu, "A 3-D spectral-element time-domain method for electromagnetic simulation," *IEEE Trans. Microw. Theory Tech.*, Vol. 55, No. 5, 983–991, May 2007.
13. Mohammadian, A. H., V. Shankar, and W. F. Hall, "Computation of electromagnetic scattering and radiation using a time-domain finite-volume discretization procedure," *Computer Physics Communications*, Vol. 68, No. 1–3, 175–196, Nov. 1991.
14. Nedelec, J. C., "Mixed finite elements in \mathbb{R}^3 ," *Numerische Mathematik*, Vol. 35, No. 3, 315–341, 1980.
15. Cohen, G. and M. Duruffe, "Non spurious spectral-like element methods for Maxwell's equations," *J. Comput. Math.*, Vol. 25, No. 3, 282–300, 2007.
16. Wang, X. and K. Bathe, "Displacement/pressure based mixed finite element formulations for acoustic UID-structure interaction problems," *Intl. J. Numer. Method. Eng.*, Vol. 40, No. 11, 2001–2017, 1997.
17. Liu, Q. H., "The PSTD algorithm: A time-domain method requiring only two cells per wavelength," *Microwave Opt. Technol. Lett.*, Vol. 15, No. 3, 158–165, Jun. 1997.
18. *Wavenology EM User's Manual*, Wave Computation Technologies, Inc., 2009.